Model Reduction of Highly Viscous, Non-isothermal Fluids with Free Surface Using Perturbation Theory

Edmond Skeli, Dirk Weidemann, Klaus Panreck,

Institut für Systemdynamik und Mechatronik, FH Bielefeld, Interaktion 1, 33619 Bielefeld
{edmond.skeli,dirk.weidemann,klaus.panreck}@fh-bielefeld.de

SNE 32(2), 2022, 93-101, DOI: 10.11128/sne.32.tn.10606
Received: 2020-11-10 (selected ASIM SST 2020 Postconf. Publication; Revised: 2022-05-02; Accepted: 2022-05-15
SNE - Simulation Notes Europe, ARGESIM Publisher Vienna, ISSN Print 2305-9974, Online 2306-0271, www.sne-journal.org

Abstract. To improve energy efficiency, the process engineering industry is increasingly tending towards an application of model-based control and diagnosis approaches. Consequently, mathematical models are required that, on the one hand, describe the technical process with sufficient accuracy, but on the other hand do not require too much computational effort. In this regard, the reduction of a model describing the behaviour of a highly viscous, non-isothermal fluid with a free surface is considered. The fluid is modelled by a system of partial differential equations. This system includes both the Navier-Stokes equations and the thermal energy equation describing the temperature behaviour. Using perturbation theory it is shown that the velocities and the temperature of the fluid can be modelled by two reduced models, denoted as submodels. The first submodel is used to calculate the flow dynamics, while the second submodel determines the thermal behaviour.

Introduction

In this paper, the inflow of a highly viscous, non-isothermal fluid into the gap between two counter-rotating cylinders is considered. Note that two conditions have to be taken into account. First, the gap is initially empty and only fills with the fluid over time, so that the inflow of the fluid is a transient process modelled by a system of partial differential equations. This system includes both the time-dependant, incompressible Navier-Stokes equations and the thermal energy equation describing the temperature behaviour. Second, a bulge forms in front of the gap during filling, the size of which changes over time until a steady state is reached. Since the temporal change of the bulge is not known in advance, the numerical solution of the system of partial differential equations simultaneously requires the determination of the fluid boundary. In the following, the fluid boundary, i.e. the surface of the fluid adjacent to the surrounding air, is also referred to as free surface.

A suitable approach to solve time-dependant, incompressible Navier-Stokes equations with a free surface is the Marker and Cell (MAC) method introduced by Harlow and Welch in [1]. Amsden and Harlow simplified the MAC method in [2] by decoupling the velocity and pressure calculations. Furthermore, in [3, 4] the MAC method is adapted for three spatial dimensions. Using the MAC method an approach to determine the free surface of a highly viscous, non-isothermal fluid entering the gap between two counter-rotating cylinders is proposed in [5]. However, it is not possible to apply it for model-based control or diagnostic approaches due to the high computational effort involved.

In order to decrease the computational effort, it is reasonable to reduce the mathematical model appropriately. Normalising the partial differential equations yields two individual time constants. These time constants allow a qualitative assessment of the transient behaviour of the velocities and the temperature, cf. [6, 7]. Using perturbation theory (cf. [8, 9]), it can be shown that the velocities and temperature of the fluid evolve on different time scales, suggesting that two reduced models, i.e. a fast and a slow submodel, can be used. The fast submodel is applied to calculate the velocities of the fluid, assuming that the fluid temperature does not change during this calculation. In contrast, the slow submodel is used to calculate the temperature, with the steady-state velocity values being determined from a system of algebraic equations.

In section 1, the mathematical model of the fluid, i.e. the system of partial differential equations consisting of Navier-Stokes equations and the thermal energy equation, is converted into a normalised form so that two individual time constants can be determined. Each of the two time constants can be used as normalisation parameter, resulting in either a fast or a slow submodel using perturbation theory, cf. Section 2. A brief presentation of the spatial discretisation and the marker and cell (MAC) method is given in Section 3 and Section 4, respectively. The solution procedure is outlined in Section 5. Finally, the numerical simulation results calculated using the reduced model are presented and compared with the results of the full model in Section 6.

1 Normalising the Model Equations

The spatio-temporal evolution of the velocities as well as the pressure of the highly-viscous, non-isothermal fluid is modelled by incompressible Navier-Stokes equations

$$\frac{\partial u}{\partial t}+u\frac{\partial u}{\partial x}+v\frac{\partial u}{\partial y}=-\frac{1}{\rho}\frac{\partial p}{\partial x}+\frac{\eta}{\rho}\left(\frac{\partial^2 u}{\partial x^2}+\frac{\partial^2 u}{\partial y^2}\right), \quad (1)$$

$$\frac{\partial v}{\partial t}+u\frac{\partial v}{\partial x}+v\frac{\partial v}{\partial y}=-\frac{1}{\rho}\frac{\partial p}{\partial y}+\frac{\eta}{\rho}\left(\frac{\partial^2 v}{\partial x^2}+\frac{\partial^2 v}{\partial y^2}\right), \quad (2)$$

$$0=\frac{\partial u}{\partial x}+\frac{\partial v}{\partial y} \quad (3)$$

with initial and boundary conditions

$$\mathbf{u}(\zeta,0)=\mathbf{u}_0(\zeta) \qquad \forall\zeta\in\Gamma, \quad (4)$$

$$\mathbf{u}(\zeta,t)=\mathbf{h}(\zeta,t) \qquad \forall(\zeta,t)\in\partial\Gamma\times[0,t_e], \quad (5)$$

where u, v represent the velocities in x-, y-direction, respectively.

In the following, $\mathbf{u}=(u,v)^T:\Gamma\times\mathbb{R}_{(+)}\to\mathbb{R}^2$ denotes the vector of fluid velocities, $\mathbf{u}_0(\zeta)\in\mathbb{R}^2$ the initial conditions and $\mathbf{h}:\partial\Gamma\times\mathbb{R}_{(+)}\to\mathbb{R}^2$ the boundary conditions, where $\Gamma\subset\mathbb{R}^2$ is the domain and $\partial\Gamma$ the boundary of the domain. Furthermore, $p:\Gamma\times\mathbb{R}_{(+)}\to\mathbb{R}$ is the pressure, $\rho\in\mathbb{R}$ the density, and $\eta(T)\in\mathbb{R}$ the viscosity.

The spatio-temporal evolution of the temperature is given by

$$\rho C_p\left(\frac{\partial T}{\partial t}+u\frac{\partial T}{\partial x}+v\frac{\partial T}{\partial y}\right)=\lambda\left(\frac{\partial^2 T}{\partial x^2}+\frac{\partial^2 T}{\partial y^2}\right)+2\eta\left(\frac{\partial u}{\partial x}\right)^2+\eta\left(\frac{\partial u}{\partial y}+\frac{\partial v}{\partial x}\right)^2+2\eta\left(\frac{\partial v}{\partial y}\right)^2, \quad (6)$$

where $T:\Gamma\times\mathbb{R}_{(+)}\to\mathbb{R}$ represents the temperature and $C_p,\lambda\in\mathbb{R}$ are the specific heat capacity and the thermal conductivity. Let the corresponding initial and boundary conditions be given by

$$T(\zeta,0)=T_0(\zeta) \qquad \forall\zeta\in\Gamma, \quad (7)$$

$$T(\zeta,t)=d(\zeta,t) \qquad \forall(\zeta,t)\in\partial\Gamma\times[0,t_e] \quad (8)$$

with $T_0(\zeta),d(\zeta,t)\in\mathbb{R}$.

Normalisation of the variables results in

$$u_n=\frac{u}{\bar{u}}, \quad v_n=\frac{v}{\bar{u}}, \quad \Pi_{px}=\frac{h^2}{\bar{u}\eta}\frac{\partial p}{\partial x}, \quad \Pi_{py}=\frac{h^2}{\bar{u}\eta}\frac{\partial p}{\partial y}, \quad x_n=\frac{x}{L}, \quad y_n=\frac{y}{h}, \quad t_n=\frac{t}{\bar{t}}, \quad T_n=\frac{T}{\bar{T}}, \quad \eta_n=\frac{\eta}{\bar{\eta}}, \quad (9)$$

where u_n, v_n, Π_{nx}, Π_{ny}, x_n, y_n represent the normalised velocities, gradients of the pressure, coordinates and t_n, T_n, η_n represent the normalised time, temperature, and viscosity.

Using the normalised variables from (9), the system of partial differential equations, which includes both the Navier-Stokes equations and the thermal energy equation, can be converted to

$$\frac{t_\eta}{\bar{t}}\frac{\partial u_n}{\partial t_n}=h_1(t_n,\mathbf{r}_n,\mathbf{u}_n,p,T_n), \quad (10)$$

$$\frac{t_\eta}{\bar{t}}\frac{\partial v_n}{\partial t_n}=h_2(t_n,\mathbf{r}_n,\mathbf{u}_n,p,T_n), \quad (11)$$

$$0=h_\nabla(\mathbf{r}_n,\mathbf{u}_n), \quad (12)$$

$$\frac{\tau_\lambda}{\bar{t}}\frac{\partial T_n}{\partial t_n}=h_3(t_n,\mathbf{r}_n,\mathbf{u}_n,p,T_n) \quad (13)$$

with $\mathbf{r}_n=[x_n,y_n]^T$, $\mathbf{u}_n=[u_n,v_n]^T$ and

$$h_1(t_n,\mathbf{r}_n,\mathbf{u}_n,p,T_n)=-Re\left(\frac{h}{L}u_n\frac{\partial u_n}{\partial x_n}+v_n\frac{\partial u_n}{\partial y_n}\right)-\Pi_{px}+\eta_n\left(\left(\frac{h}{L}\right)^2\frac{\partial^2 u_n}{\partial x_n^2}+\frac{\partial^2 u_n}{\partial y_n^2}\right), \quad (14)$$

$$h_2(t_n,\mathbf{r}_n,\mathbf{u}_n,p,T_n)=-Re\left(\frac{h}{L}u_n\frac{\partial v_n}{\partial x_n}+v_n\frac{\partial v_n}{\partial y_n}\right)-\Pi_{py}+\eta_n\left(\left(\frac{h}{L}\right)^2\frac{\partial^2 v_n}{\partial x_n^2}+\frac{\partial^2 v_n}{\partial y_n^2}\right)$$

$$h_\nabla(\mathbf{r}_n,\mathbf{u}_n)=\frac{\bar{u}}{h}\left(\frac{h}{L}\frac{\partial u_n}{\partial x_n}+\frac{\partial v_n}{\partial y_n}\right), \quad (15)$$

$$h_3(t_n,\mathbf{r}_n,\mathbf{u}_n,p,T_n) = -Gr\left(u_n\frac{\partial T_n}{\partial x_n}+v_n\frac{L}{h}\frac{\partial T_n}{\partial y_n}\right) + \left(\left(\frac{h}{L}\right)^2\frac{\partial^2 T_n}{\partial x_n^2}+\frac{\partial^2 T_n}{\partial y_n^2}\right)+2\eta_n Br\left(\frac{h}{L}\right)^2\left(\frac{\partial u_n}{\partial x_n}\right)^2 + \eta_n Br\left(\frac{\partial u_n}{\partial y_n}+\frac{h}{L}\frac{\partial v_n}{\partial x_n}\right)^2+2\eta_n Br\left(\frac{\partial v_n}{\partial y_n}\right)^2. \tag{16}$$

Here

$$Re=\frac{\rho h\bar{u}}{\bar{\eta}},\qquad Br=\frac{\bar{\eta}\bar{u}^2}{\lambda\bar{T}},\qquad Gr=\frac{\bar{u}h^2}{aL} \tag{17}$$

denote the Reynolds, Brinkmann and Graetz numbers and

$$t_\eta=\frac{\rho h^2}{\bar{\eta}},\qquad \tau_\lambda=\frac{h^2\rho C_p}{\lambda} \tag{18}$$

the viscous relaxation time and the conductive thermal equilibrium time, respectively.

2 Model Reduction using Perturbation Theory

In the following, the relation between the two time constants given in (18) will be considered in more detail, as these provide information about the transient behaviour of the velocities and temperature. Dividing the viscous relaxation time by the conductive thermal equilibrium time yields

$$\frac{t_\eta}{\tau_\lambda}=\frac{\frac{\rho h^2}{\bar{\eta}}}{\frac{h^2\rho C_p}{\lambda}}=\frac{\lambda}{\bar{\eta}C_p}. \tag{19}$$

and shows that

$$\tau_\lambda >> t_\eta \tag{20}$$

holds due to the high viscosity of the fluid. Speaking in physical terms, the relation (20) indicates that the dynamics of the velocities is much faster than the dynamics of the temperature.

Optionally, either $\bar{t}=t_\eta$ or $\bar{t}=\tau_\lambda$ can be used as the normalisation constant. The following two subsections discuss how the equations (10)-(13) change when $\bar{t}=t_\eta$ or $\bar{t}=\tau_\lambda$ is chosen.

2.1 Viscous Relaxation Time as Normalisation Constant

If t_η is chosen as the normalisation constant, $t_\eta/\bar{t}=t_\eta/t_\eta=1$ and $\tau_\lambda/\bar{t}=\tau_\lambda/t_\eta$ follow for the factors on the left-hand side of (10), (11), and (13) such that the normalised Navier-Stokes equations are of the form

$$\frac{\partial u_n}{\partial t_n}=h_1(t_n,\mathbf{r}_n,\mathbf{u}_n,p,T_n), \tag{21}$$

$$\frac{\partial v_n}{\partial t_n}=h_2(t_n,\mathbf{r}_n,\mathbf{u}_n,p,T_n), \tag{22}$$

$$0=h_\nabla(\mathbf{r}_n,\mathbf{u}_n). \tag{23}$$

Furthermore, choosing $t_\eta/\tau_\lambda=\varepsilon$ with $\varepsilon\ll 1$ as perturbation parameter and multiplying the thermal energy equation (13) by ε results in

$$\frac{\partial T_n}{\partial t_n}=\varepsilon h_3(t_n,\mathbf{r}_n,\mathbf{u}_n,p,T_n)=0. \tag{24}$$

The model given by (21)-(23) is referred to as fast submodel. It will be applied to compute the velocities when a change in momentum occur. Since the temperature does not change significantly over t_η, the partial differential equation (13) does not have to be solved. Rather, as indicated by (24), the temperature can be regarded as being approximately constant.

2.2 Conductive thermal Equalization Time as Normalisation Constant

In contrast to Section 2.1, the choice of τ_λ as normalization constant leads to a system of singularly perturbed partial differential equations

$$\varepsilon\frac{\partial u_n}{\partial t_n}=h_1(t_n,\mathbf{r}_n,\mathbf{u}_n,p,T_n), \tag{25}$$

$$\varepsilon\frac{\partial v_n}{\partial t_n}=h_2(t_n,\mathbf{r}_n,\mathbf{u}_n,p,T_n), \tag{26}$$

$$0=h_\nabla(\mathbf{r}_n,\mathbf{u}_n), \tag{27}$$

$$\frac{\partial T_n}{\partial t_n}=h_3(t_n,\mathbf{r}_n,\mathbf{u}_n,p,T_n), \tag{28}$$

where ε is defined as described above. Assuming $\varepsilon\to 0$ the Navier-Stokes equations simplify to

$$0=h_1(t_n,\mathbf{r}_n,\mathbf{u}_n,p,T_n), \tag{29}$$

$$0=h_2(t_n,\mathbf{r}_n,\mathbf{u}_n,p,T_n), \tag{30}$$

$$0=h_\nabla(\mathbf{r}_n,\mathbf{u}_n). \tag{31}$$

The model given by (28)-(31) is referred to as slow submodel and is used to calculate the fluid temperature. When calculating the temperature, the velocities are not to be interpreted as differential, but as algebraic states that have to be adjusted so that the algebraic conditions (29)-(31) are satisfied.

2.3 Hybrid Model

In contrast to the approach in [5], which calculates the inflow of the fluid into the gap using the full model, i.e. the partial differential equations (1)-(6), the approach presented in this paper uses the reduced model equations (21)-(23) and (28)-(31). It can be shown that the computation time decreases significantly by employing the reduced models.

The slow submodel is used as long as no momentum changes act on the fluid. Whereas the fast submodel is used until the velocities of the fluid are stationary. Interpreting an momentum change as event e_{mc} and the occurrence of the stationary velocities as event e_{sv}, the fluid can be modelled by the hybrid automaton shown in figure 1.

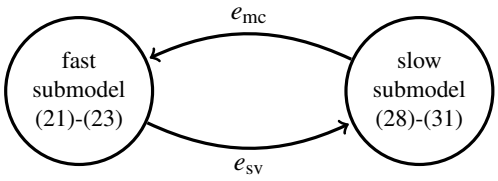

Figure 1: Reduced model as hybrid automaton.

3 Spatial Discretisation

Regarding the use of a numerical method to solve the partial differential equations, a suitable spatial discretisation is required. As depicted in figure 2 the velocities are calculated at the middle of the vertical and horizontal edges of the discretisation gird, whereas the pressure and the temperature are calculated at the centre of a cell. This grid, referred to as staggered gird, is chosen since it allows for the solution to have a tight coupling between the pressure and the velocity.

The partial derivatives of first order can be approximated by

$$D^x f_{i,j} = \frac{f_{i,j+1} - f_{i,j-1}}{2\Delta x}, \tag{32}$$

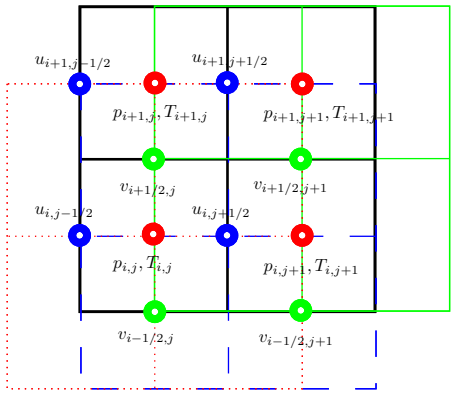

Figure 2: Staggered grid and calculation nodes.

$$D^x_- f_{i,j} = \frac{f_{i,j} - f_{i,j-1}}{\Delta x}, \tag{33}$$

$$D^x_+ f_{i,j} = \frac{f_{i,j+1} - f_{i,j}}{\Delta x}, \tag{34}$$

and partial derivatives of second order by

$$K^x f_{i,j} = \frac{f_{i,j+1} - 2f_{i,j} + f_{i,j-1}}{(\Delta x)^2}, \tag{35}$$

where f represents either u, v, p or T, $n_1, n_2 \in \mathbb{R}$ denote the number of discretisation lines in x- and y- direction, $i = 1,2,...,n_1$ and $j = 1,2,...,n_2$ are the indices of the cells, and Δx is the discretisation step in x-direction. The operators D^y, D^y_-, D^y_+ and K^y are defined analogously with $\Delta y = f_{\Delta y}(x)$ being the varying step size in y-direction of the curvilinear discretisation grid depicted in figure 3.

The curvilinear discretisation gird has the advantage over a rectangular grid that all points are within the domain Γ. Thus, leading to less computational effort. However, a meaningful use of the curvilinear grid is only possible with sufficiently large radii, as there is a risk of inaccurate calculation with small radii. Note that even with the curvilinear discretisation grid, the velocities are still computed at the centre of the cell edge, while pressure and temperature are computed at the centre of the cell, with the cell contour shown in 3.

Choosing this discretisation the fast system (21)-(23) can be formulated as

$$I\dot{\mathbf{u}}(t) = K(\mathbf{u})\mathbf{u}(t) - Bp(t) + \mathbf{f}(\mathbf{u}(t), p(t)), \tag{36}$$

$$0 = B^T \mathbf{u}(t) \tag{37}$$

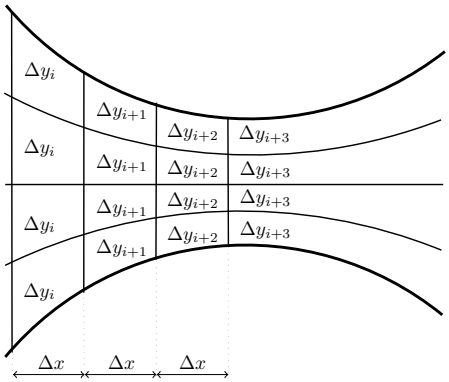

Figure 3: Curvilinear grid.

and the slow system (28)-(31) as

$$0 = K(\mathbf{u})\mathbf{u}(t) - Bp(t) + \mathbf{f}(\mathbf{u}(t), p(t)), \tag{38}$$

$$0 = B^T\mathbf{u}(t), \tag{39}$$

$$I\dot{T}(t) = K_T(\mathbf{u})T(t) + D(\mathbf{u}) + g(T(t)), \tag{40}$$

with I being the identity matrix and $B = [D^x_+, D^y_+]^T$ the discrete divergence operator,

$$K(\mathbf{u}) = \begin{bmatrix} K_1 + N_1(\mathbf{u}) & 0 \\ 0 & K_2 + N_1(\mathbf{u}) \end{bmatrix}$$

with $K_1 = K_2 = K^x + K^y$ representing the linear (diffusion) and

$$N(\mathbf{u}) = \begin{bmatrix} N_1(\mathbf{u}) \\ N_2(\mathbf{u}) \end{bmatrix} = \begin{bmatrix} u_{i,j+1/2}D^x + v^*_{i,j+1/2}D^y \\ u^*_{i+1/2,j}D^x + v_{i+1/2,j}D^y \end{bmatrix}$$

the non-linear (convection) terms. The velocities $u^*_{i+1/2,j}$ and $v^*_{i,j+1/2}$ are averaged velocities defined by

$$u^*_{i+1/2,j} = \frac{1}{4}\left(u_{i,j-1/2} + u_{i,j+1/2} + u_{i+1,j+1/2} + u_{i+1,j-1/2}\right),$$

$$v^*_{i,j+1/2} = \frac{1}{4}\left(v_{i-1/2,j} + v_{i+1/2,j} + v_{i+1/2,j+1} + v_{i-1/2,j+1}\right).$$

Moreover, $\mathbf{f}(\mathbf{u}(t), p(t))$ and $g(T(t))$ depend on the boundary conditions such that these functions have to be adapted according to the modification of the free-surface, cf. Section 4. Finally, the operators for the temperature calculation are given by

$$D(\mathbf{u}) = 2\eta((D^x_+u)^2 + \frac{1}{\eta}(D^y_+u + D^x_+v)^2 + (D^y_+v)^2)$$

and $K_T(\mathbf{u}) = (K_1 + N_T(\mathbf{u}))$ with

$$N_T(\mathbf{u}) = \frac{u_{i,j-1/2} + u_{i,j+1/2}}{2}D^x + \frac{v_{i-1/2,j} + v_{i+1/2,j}}{2}D^y.$$

4 Determination of the free Surface

The MAC method which was introduced by Harlow and Welch in [1] is implemented to determine the free surface of the fluid. According to the MAC method, massless particles are used to mark the fluid cells, i.e. each cell of the discretisation grid that includes at least one massless particle is part of the area containing the fluid. Thus, the massless particles are referred to as markers. If one or more empty cells of the discretisation grid are adjacent to a cell filled with fluid, the free surface passes through the fluid cell. Such constellations are shown in figure 4 and figure 5, respectively.

Note that normal and tangential stresses on a free surface of an incompressible fluid are equal to zero (cf. [10, 11]). Thus, the boundary values of the velocities and the pressure on the free surface have to satisfy

$$\frac{p}{\rho} = 2\frac{\eta}{\rho}\left[n_x n_x \frac{\partial u}{\partial dx} + n_x n_y\left(\frac{\partial u}{\partial y} + \frac{\partial v}{\partial x}\right) + n_y n_y \frac{\partial v}{\partial y}\right], \tag{41}$$

$$\left[2n_x m_x \frac{\partial u}{\partial x} + 2n_y m_y \frac{\partial v}{\partial y}\right] = -(n_x m_y + n_y m_x)\left(\frac{\partial u}{\partial y} + \frac{\partial v}{\partial x}\right), \tag{42}$$

where $\mathbf{n} = (n_x, n_y)$ is the normal and $\mathbf{m} = (m_x, m_y) = (n_y, -n_x)$ is the tangential vector.

The following two examples serve as an explanation for determining the boundary conditions. In figure 4 the marked cell at the bottom left is only adjacent to a single free cell above it. Consequently, the normal component n_x is zero or at least very small, such that (41), (42) simplify to

$$p_{i,j} - 2\eta(D^y_+v) = 0, \tag{43}$$

$$D_+^y u = -D_+^x v. \tag{44}$$

The pressure $p_{i,j}$ and the velocity $v_{i+1/2,j}$ are calculated with (43) and (44), respectively.

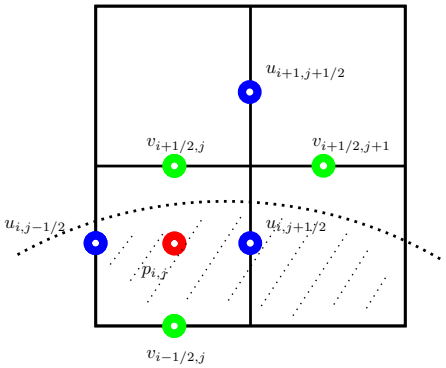

Figure 4: Marked cell with a free adjacent cell.

In figure 5, two empty cells are adjacent to the marked cell, in such a scenario it is assumed that the normal vector has an angle of 45 degrees, i.e., points upwards to the right. In this case, (41), (42) simplify to

$$p_{i,j} - \eta(D_+^y u + D_+^x v) = 0 \tag{45}$$

and

$$D_+^x u - D_+^y v = 0. \tag{46}$$

The pressure $p_{i,j}$ is calculated based on (45), whereas the velocities are set to $u_{i,j+1/2} = u_{i,j-1/2}$ and $v_{i+1/2,j} = v_{i-1/2,j}$ such that (46) is met. Further scenarios can be found in [2].

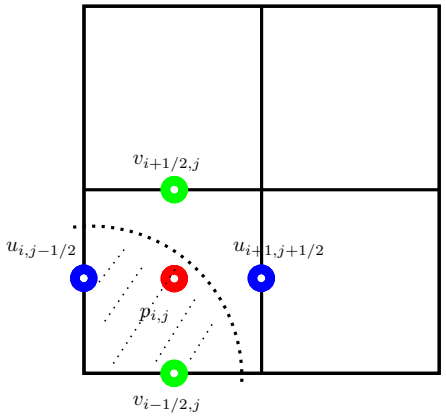

Figure 5: Marked cell with two free adjacent cells.

5 Solution Procedure

The solution procedure includes both the calculation of the two submodels and the switching between the submodels.

5.1 Fast Submodel

Regarding the calculation of the fast submodel (36)-(37), the projection method of Chorin is implemented according to the algorithm proposed in [12]. Note that the temperature values are kept constant such that $T^k = T^{k-1}$ holds. The algorithm contains:

- Perform a semi-implicit time discretisation of (36)-(37) resulting in

$$\frac{\mathbf{u}^k - \mathbf{u}^{k-1}}{\Delta t} = K(\mathbf{u}^{k-1})\mathbf{u}^{k-1} - Bp^k + \mathbf{f}^k, \tag{47}$$

$$0 = B^T \mathbf{u}^k \tag{48}$$

  with Δt being the step size and k the current time instant.

- Decouple the pressure from the momentum equation (47) and calculate the pseudo velocities $\tilde{\mathbf{u}}$ by solving

$$\frac{\tilde{\mathbf{u}} - \mathbf{u}^{k-1}}{\Delta t} = K(\mathbf{u}^{k-1})\mathbf{u}^{k-1} + \mathbf{f}^k. \tag{49}$$

  for $\tilde{\mathbf{u}}$.

- Calculate the pressure by solving

$$\Delta t B^T B p^k = B^T \tilde{\mathbf{u}} \tag{50}$$

  for p^k and calculate the corrected velocities according to

$$\mathbf{u}^k = \tilde{\mathbf{u}} - \Delta t B p^k. \tag{51}$$

5.2 Slow Submodel

The calculation of the slow subsystem (38)-(40) is done according to the following steps:

- Perform a semi-implicit time discretisation of (40) resulting in

$$\frac{T^k - T^{k-1}}{\Delta t} = K_T(\mathbf{u}^{k-1})T(t) + D(\mathbf{u}^{k-1}) + g(T^{k-1}) \tag{52}$$

and calculate the temperature by solving (52) for T^k.

- Decouple the velocities from the pressure and calculate the pseudo-velocies $\tilde{\mathbf{u}}$ by solving the non-linear system of steady, spatially discretised Navier-Stokes equations given by

$$\mathbf{0} = K(\tilde{\mathbf{u}})\tilde{\mathbf{u}} + \mathbf{f}^k. \tag{53}$$

- Determine the pressure by solving

$$\Delta t B^T B p^k = B^T \tilde{\mathbf{u}} \tag{54}$$

for p^k.

- Correct the velocities according to

$$\mathbf{u}^k = \tilde{\mathbf{u}} - \Delta t B p^k. \tag{55}$$

5.3 Switching Submodels

As long as there are no momentum changes, the slow submodel is used. A change in momentum, indicated by event e_{mc} (see figure 1), is assumed to take place when the fluid enters a cell of the discretisation grid at time t that was previously at time $t-1$ not filled with fluid. Such a scenario is shown in figure 6, where the left plot shows the cell occupancy at time $t-1$ and the right plot shows the occupancy at time t.

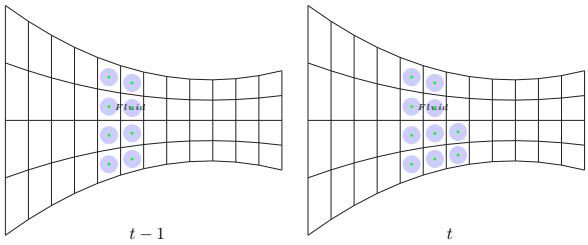

Figure 6: Cell occupancy at $t-1$ and t.

As soon as the occupied cells do not change and the velocity of the fluid in these cells is stationary, indicated by event e_{sv}, the slow submodel is used. The plot on the left side of figure 7 implies that with constant cell occupancy, the velocities differ at times $t-1$ and t. In this case, it is imperative to continue using the fast submodel. In contrast, stationary velocities are present in the plot on the right-hand side, so that a submodel switch takes place.

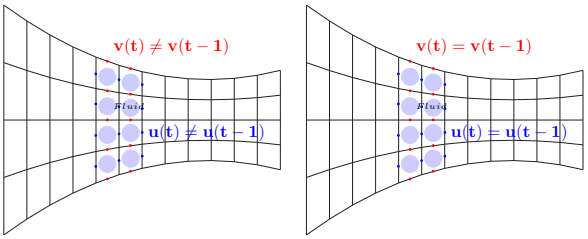

Figure 7: Stationay vs. transient velocities with constant cell occupancy.

6 Simulation Results

Though the complete evolution of all quantities, i.e. velocities, the pressure, and temperature over time have been calculated, in the following only the temperature and the velocity in x-direction at the time t_{ss} are presented, where t_{ss} indicates the time at which the steady state is reached. Note the the computations takes about 10 hours for the full model but only approx. 10 min. for the reduced model.

The initial temperature field in a cross-section located in the middle of the cylinders is depicted in figure 8. As can be seen in figure 8 the initial temperature of the fluid is 425 K while the ambient temperature is 400 K and the temperature of the cylinders is 433 K.

Figure 9 shows the calculated temperature field of the fluid in a cross-section using the full model. In contrast, the temperature field calculated with the reduced model is shown in figure 10. Although there are differences between the temperature field determined by the full model and the temperature field calculated using the reduced model, the reduced model shows a behaviour similar to that of the full model in terms of quality and quantity. Comparing the initial temperature field with either figure 9 or 10, one can see from the temperature change which place the fluid has occupied in the steady state.

For the velocity in the x-direction, a similar characteristic can be seen as for the temperature, with the initial velocity field being shown in figure 13. Only minor differences exist between the results of the full model, shown in Figure 12, and those calculated with the reduced model (see Figure 13). Note that some negative velocities occur in the gap. These negative values result from the high pressure gradient which occurs when the fluid enters the gap, so that the pressure gradient counteracts the flow, resulting in a backflow of the fluid such that a limited bulging occurs in front of the gap. In addition,

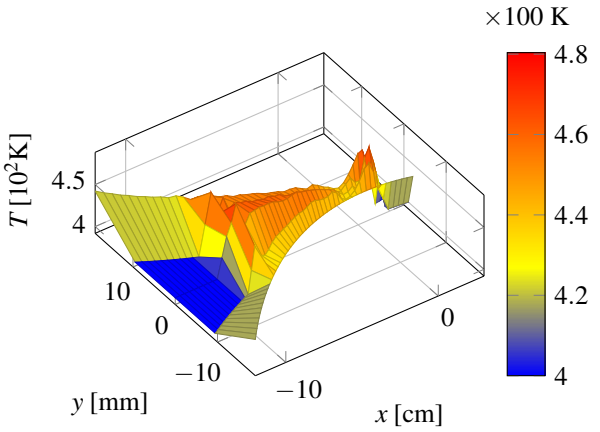

Figure 9: Temperature field in a cross-section (full model).

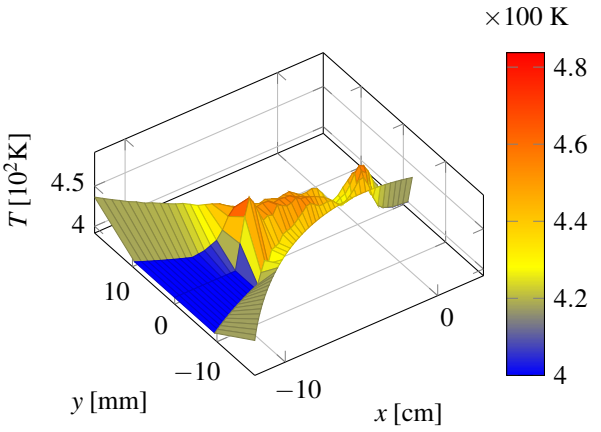

Figure 10: Temperature field in a cross-section (reduced model).

the pressure in some gap sections decreases continuously. In these sections, the pressure gradient acts in positive x-direction, which leads to increased velocities as can be seen in figure 12 as well as in figure 13.

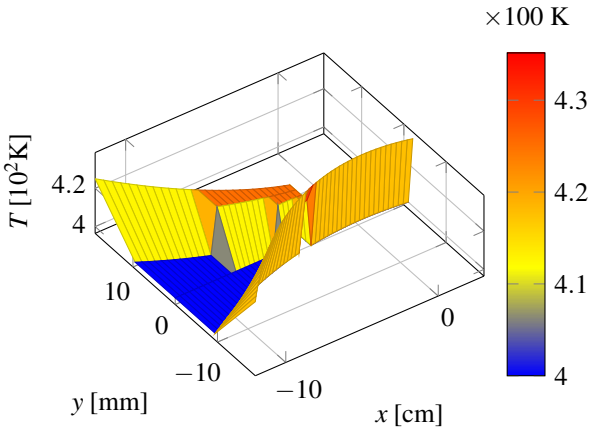

Figure 8: Initial temperature field in a cross-section.

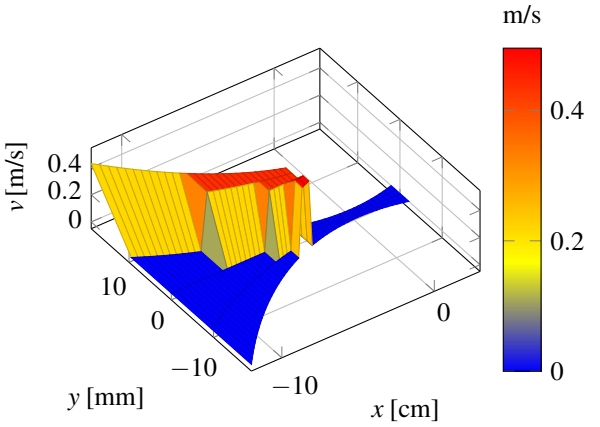

Figure 11: Initial velocity in x-direction in a cross-section.

7 Conclusion

The simulation of models describing the behaviour of highly viscous, non-isothermal fluids is usually associated with a high computational effort. Thus, such models are neither used for model-based control methods nor for model-based diagnosis. Using perturbation theory, however, it can be shown that the velocities and the temperature of the fluid evolve on different time scales, which indicates that two reduced models, i.e. a fast and a slow submodel, can be applied. As long as the fast submodel is used, the velocities are calculated assuming a constant temperature field, since the latter quantity evolves on a lesser time scale. In contrast to the fast submodel, the slow submodel calculates the temperature assuming steady-state velocities evolving on a faster time scale. A comparison of the results calculated with the different models (full model vs. reduced model) shows a high level of agreement. Although the difference in computational effort is significantly (approx. 10 hours for the full model vs. approx. 10 minutes for the reduced model), further model reduction is necessary in order to use the

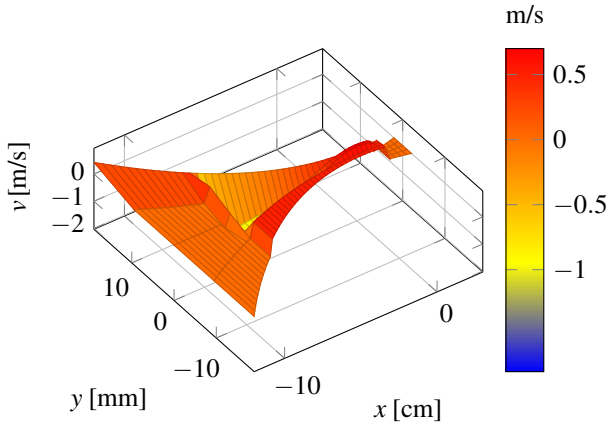

Figure 12: Velocity in x-direction in a cross-section (full model).

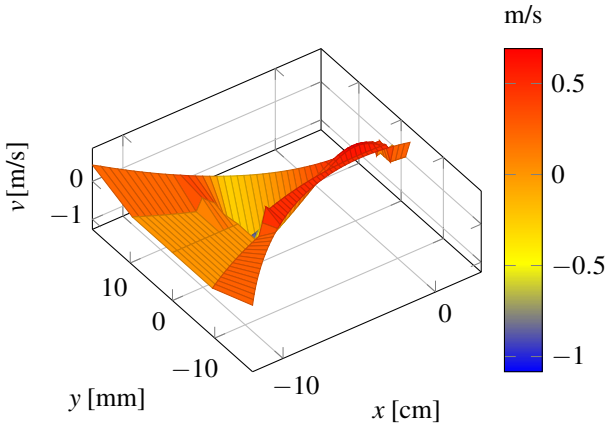

Figure 13: Velocity in x-direction in a cross-section (reduced model).

model reasonably for model-based control and diagnosis approaches.

Acknowledgement

The authors would like to thank the European Union and the federal state of North Rhine-Westphalia, Germany, for the financial support.

References

[1] Harlow, F. H., Welch J. E., *Numerical calculation of time-dependent viscous incompressible flow of fluid with free surface*, The Physics of Fluids, vol. 8, no. 12, pp. 2182–2189, 1965.

[2] Amsden, A. A., Harlow, F. H., *The smac method: A numerical technique for calculation incompressible fluid flows*, Los Alamos Scientific Laboratory, University of California, Tech. Rep., 1970.

[3] Tome, M., Filho, A., Cuminato, J. A., Mangiavacchi, N., Mc-Kee, S., *Gensmac3d: a numerical method for solving unsteady three-dimensional free surface flows*, International Journal for Numerical Methods in Fluids, vol. 37, no. 7, pp. 747–796, 2001.

[4] McKee, S., Tome, M., Ferreira, V., Cuminato, J., Castelo, A., Sousa, F., Mangiavacchi, N., *The mac method*, Computer & Fluids, vol. 37, no. 8, pp. 907–930, 2008.

[5] Harder, D., Skeli, E., Weidemann, D., *Modelling and simulation of high-viscosity, non iso-thermal fluids with a free surface*, in Proc. of the 15th Conference on Informatics, Automation, and Robotics (ICINCO), pp. 557–563, 2018.

[6] Lichte, B., *Verläßliche und effiziente Simulation physikalisch-technischer Systeme durch Nutzung von Fachwissen*, Shaker Verlag, 2006.

[7] Panreck, K., *Verkopplungsorientierte Modellbildung und Simulation instationärer Extrusionsprozesse*, Dissertation, Univ. Paderborn, 1995.

[8] Kokotovic, P. V., *Singular perturbation techniques in control theory*, in Singular Perturbations and Asymptotic Analysis in Control Systems, Kokotovic, P. V., Bensoussan, A., Blankenship, G. L. (Editoren), pp. 1–55, Springer, 1987.

[9] Verhulst, F., *Methods and applications of singular perturbations - Boundary layers and multiple timescale dynamics*, Springer, 2005.

[10] Hirt, C. W., Shannon, J. P., *Free-surface stress conditions for incompressible-flow calculations*, Journal of Computational Physics, vol. 2, no. 4, pp. 403–411, 1968.

[11] Nichols, B. D., Hirt, C. W., *Improved free surface boundary conditions for numerical incompressible-flow calculations*, Journal of Computational Physics, vol. 8, no. 3, pp. 434–448, 1971.

[12] Weickert, J., *Applications of the theory of differential-algebraic equations to partial differential equations of fluid dynamics*, Dissertation, TU Chemnitz, 1997.